Experimental validation of a TRC model for a double U-tube borehole with two independent circuits

by

Bruno Marcotte

and

Michel Bernier[1], PE, Ph.D.

Polytechnique Montréal

Department of Mechanical Engineering

2500 chemin de Polytechnique

Montréal, Canada, H3T 1J4

Accepted manuscript

Declarations of interest: none

[1] Corresponding author: Tel.: +1-514-340-4711; *e-mail address:* michel.bernier@polymtl.ca.

Experimental validation of a TRC model for a double U-tube borehole with two independent circuits

Abstract:

This paper presents an experimental validation of a thermal resistance and capacitance (TRC) model for double U-tube boreholes with two independent circuits. In the TRC model, the borehole cross-section is divided into four quadrants each with two nodes representing the fluid and the grout, respectively. Ground heat transfer is evaluated in each of the n vertical sections using the infinite cylindrical source analytical solution with appropriate temporal superposition. Finally, internal tube-to-tube and tube-to-borehole thermal resistances are evaluated with the multipole method. The TRC model is validated against results obtained using a small-scale borehole (90.39 cm long with a 9.45 cm diameter) positioned in a sand tank of known properties. The borehole is made of ceramic which enabled the precise positioning of thermocouples at the mid-height cross-section. Data are acquired at a high frequency (1 s) to capture transient effects. In the first set of results obtained for a quasi-steady state, isotherms over the mid-height cross-section compare favorably well with the ones obtained using the multipole method. In the other two tests, the borehole is subjected to varying inlet (flow rate and temperature) conditions. It is shown that the TRC model is in good agreement with the experimental data except when there is a severe steep change in inlet temperature or when there is no flow.

Keywords: Boreholes; thermal resistance; thermal capacitance, heat transfer, TRC model

1. Introduction

Double U-tube boreholes with two independent circuits have recently been proposed (Brischoux & Bernier, 2016; Eslami-Nejad & Bernier, 2011a, 2011b, 2012; Godefroy, 2014; Thorén, 2016). One possible application of this geometry is shown in Figure 1 where solar collectors and a heat pump are connected to a double U-tube borehole. The heat pump is connected to the U-tube formed by pipes #1 (downward flow) and #3 (upward flow) while solar collectors are linked to the U-tube formed by pipes #2 (downward flow) and #4 (upward flow). In this configuration, three modes of operation are possible: i) the borehole is used to store heat into the ground when solar energy is available and the heat pump does not operate; ii) the borehole is used to collect heat from the ground when the heat pump operates and solar collection is not possible; iii) the borehole acts as a heat exchanger between the solar collectors and the heat pump when both are operational with the excess heat transferred to the ground.

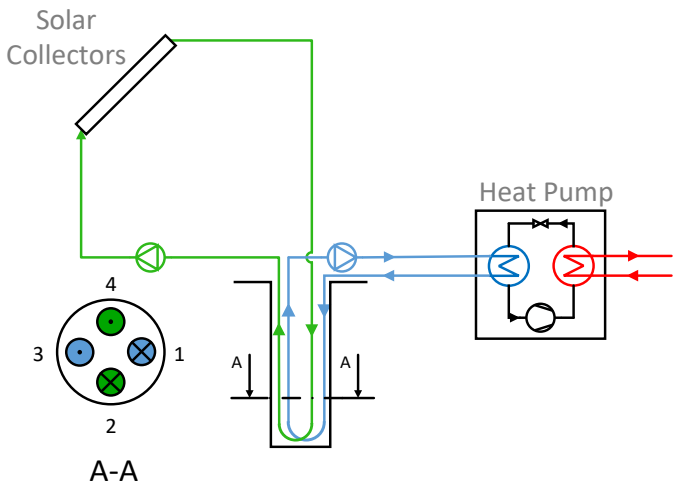

Figure 1 : Example of a double U-tube geometry with two independent circuits

This geometry has many advantages and a numerical model to predict its thermal performance enables further feasibility studies of this configuration. This paper aims at providing such a model based on the so-called Thermal Resistance Capacitance (TRC) approach. The model is then validated against high frequency data obtained using the small-scale borehole test facility developed by Salim-Shirazi and Bernier (2014).

2. Literature review

Geothermal boreholes operate under various operating conditions but are rarely operating in a pure steady-state where temperatures in the borehole (from the fluid to the borehole wall) remain constant. Nonetheless, steady-state conditions can be approached when the fluid temperature and flow rate do not change significantly with time. Steady-state conditions are typically modeled using a constant borehole thermal resistance, R_b. As mentioned by Javed and Spitler (2016, 2017), the value of R_b is specific to a cross-section. For a given heat transfer rate per unit length and borehole wall temperature, R_b can be used to determine the mean fluid temperature in a borehole cross-section. There are a number of ways to evaluate R_b (Javed & Spitler, 2017). Two of the most popular techniques are the shape factor method of Paul (1996) and the multipole method (Bennet et al., 1987; Claesson & Javed, 2011, 2018; Hellström, 1991).

In most cases, the cross-sectional value of R_b can be used to determine the overall mean fluid temperature in the borehole. However, for long boreholes and low flow rates, the value of R_b is adjusted (and now typically called R_b^*) to account for the thermal short-circuit between the ascending and descending pipes. Claesson and Javed (2011) proposed values for R_b^* for two borehole wall boundary conditions: uniform heat transfer rate and uniform borehole wall temperature. Eslami-Nejad and Bernier (2011a, 2011b) developed steady-state models for double U-tube boreholes for various circuitry including the case of two independent circuits (Figure 1).

Yavuzturk and Spitler (1999) were among the first to treat the pipe and grout thermal capacities when they extended the concept of g-functions to small time steps by solving numerically borehole heat transfer with a pie sector approximation for a single U-tube geometry. Xu and Spitler (2006) took a different approach with an equivalent geometry composed of a series of hollow cylinders which included the fluid thermal capacity.

Recent studies have proposed various approaches to model transient borehole behaviour. Cui et al. (2008) used a finite element model to represent a single U-tube borehole operating in transient. The proposed model is able to satisfactorily reproduce experimental data with hourly inlet condition variations. Zarrella et al. (2011a, 2011b) developed the CaRM model for standard double U-tube boreholes (one circuit feeding two descending and two ascending tubes) using a combination of thermal resistances and capacitances. Bauer et al. (2011) presented a similar approach, referred to as a TRCM model for various

types of boreholes including standard double U-tube boreholes. The proposed TRCM model was compared to a 3D finite element model with satisfactory results. Pasquier and Marcotte (2012) presented an improved version of the TRCM model for single U-tube boreholes by taking into account the thermal capacity of the fluid and pipes. Shirazi and Bernier (2013) also developed a numerical model to take into account the transient behavior of a single U-tube borehole. They used their 1-D model in annual simulations to show that neglecting borehole thermal capacity (fluid and grout) can lead to a 4-5% overestimation of heat pump energy consumption. Yang and Li (2014) proposed a numerical model consisting of a line-source in a composite medium to simulate a single U-tube borehole with short time steps. Their numerical model was validated using the sandbox data of Beier et al. (2011) for a single U-tube borehole.

Godefroy (2014) presented transient numerical models for single and double U-tube boreholes based on the TRC approach where the borehole is divided into a number of vertical elements. The model is coupled to the infinite cylindrical source analytical solution to simulate ground heat transfer. Experimental data on a single U-tube borehole was used to successfully validate the TRC model (Godefroy et al. (2016). However, as pointed out by Godefroy (2014), there are no experimental data to validate the model for double U-tube boreholes with two independent circuits.

M. De Rosa et al. (2015) presented a single U-tube numerical model called B2G based on a TRC network. The model was compared to experimental data and the Duct ground heat STorage (DST) model (Hellström, 1989) which does not account for borehole thermal capacity (De Rosa et al., 2014). Results show that the B2G model is able to reproduce experimental data for short time steps but also highlight the importance of borehole thermal capacity to assess control strategies based on the heat carrier fluid temperature. Pärisch et al. (2015) adapted the SBM (Eskilson, 1987) and DST models for short time-step simulations by adding an upstream pipe filled with the heat carrier fluid.

Rees (2015) proposed a 2-D finite volume method to simulate heat transfer inside boreholes. The model was validated for short time steps with experimental data collected at Oklahoma State University (Hern (2004) and Gentry (2007)). The author also noted the lack of experimental data available to validate borehole numerical models.

Abdelaziz and Ozudogru (2016) proposed a simplified approach based on the finite line source model for an homogeneous medium to approximate the average temperature changes expected over the cross-section

of energy piles with embeded pipes including a four pipe configuration. The pile material is transferred into an equivalent soil domain using an equivalent radius. The proposed analytical solution is validated against a finite element numerical models for energy piles with various sizes and different number of heat exchange loops.

Kramer et al. (2015) performed a series of laboratory tests on a small-scale geothermal pile in sand equipped with a U-shaped circulation tube. Temperatures recorded at different locations within the soil chamber show that heat transfer from a geothermal pile with a single U-tube can actually be approximated as an axisymmetric heat transfer process in the medium surrounding the pile.

Minaei and Maerefat (2017) developed a model based on a network of thermal resistances and capacitances for single and double U-tubes borehole. The thermal resistances are computed using the multipole method (Claesson & Javed, 2011). Only the single U-tube model could be compared to experimental data provided by Beier et al. (2011). Results from their proposed model were also compared to a finite element model with satisfactory results.

Recently, Kerme anf Fung (2020) provided a TRC model for a single U-tube borehole. The governing transient equations of the ground and grout are obtained from energy balances with thermal resistances between nodes. A fully implicit Crank-Nicolson method is used to solve the problem. Their model compared favorably well with solutions found in the literature. Their model was used to perform a series of parametric analyses on the effect of mass flow rate and grout thermal conductivity.

In her analysis of borehole thermal energy storage for solar communities, Verstraete (2013) used the modified DST model of Chapuis (2009) to simulate double U-tube boreholes with two independent circuits. However, Chapuis's simplified approach did not account for borehole thermal capacity. More recently, Lecomte and Bernier (2016) developed a model where borehole-to-borehole and tube-to-tube heat transfer within a borehole are solved using the finite line source analytical solution. With this approach, transient effects in boreholes, including double U-tube boreholes, can be evaluated. However, in its current version, the model assumes identical ground and grout thermal properties.

Two- and three-dimensional transient borehole models have been presented. For example, Rees and He (2013) and He (2012) present a 3-D numerical finite volume model with explicit representations of the ground, pipes, fluid and grout in a geometrically correct manner. Even though these models offer great

precision with their fine meshes, they are often too slow to perform annual simulations. TRC models offer a faster alternative using relatively coarse grids.

In summary, it appears that there are a number of single U-tube borehole models either for steady-state or transient conditions. There are good sets of experimental data to validate these models. Conventional double U-tubes boreholes have also been modeled successfully either in steady-state or in transient mode. However, double U-tube boreholes with two independent circuits have not been studied extensively and there is a clear lack of experimental data to validate models for this configuration. This paper attempts to alleviate these deficiencies by improving the original TRC model of Godefroy (2014) and validating it with high frequency experimental data obtained on a fully instrumented small-scale borehole.

3. TRC model

The TRC model for double U-tube boreholes with two independent circuits developed in this section is largely inspired by the work of Godefroy (2014) but with a different thermal network. As shown in Figure 2a, the borehole is discretized axially into n disks. In each disk, heat transfer is modelled with a network of thermal resistances and capacitances as shown in Figure 2d. Contrary to most TRC models who treat heat transfer from the borehole wall to the ground numerically, the proposed model uses the analytical cylindrical heat source solution to predict ground heat transfer.

As shown in Figure 2c, the borehole cross-section is divided into four identical quarters each with its own temperature, $T_{g,x,i}$ where the subscripts x and i refer to specific pipes (1 2, 3, or 4) and vertical disks (1 to n), respectively. The mean borehole wall temperature is given by $T_{b,i}$. The nodes identified as $T_{f,x,i}$ represent the mean fluid temperature for a specific pipe and vertical disk.

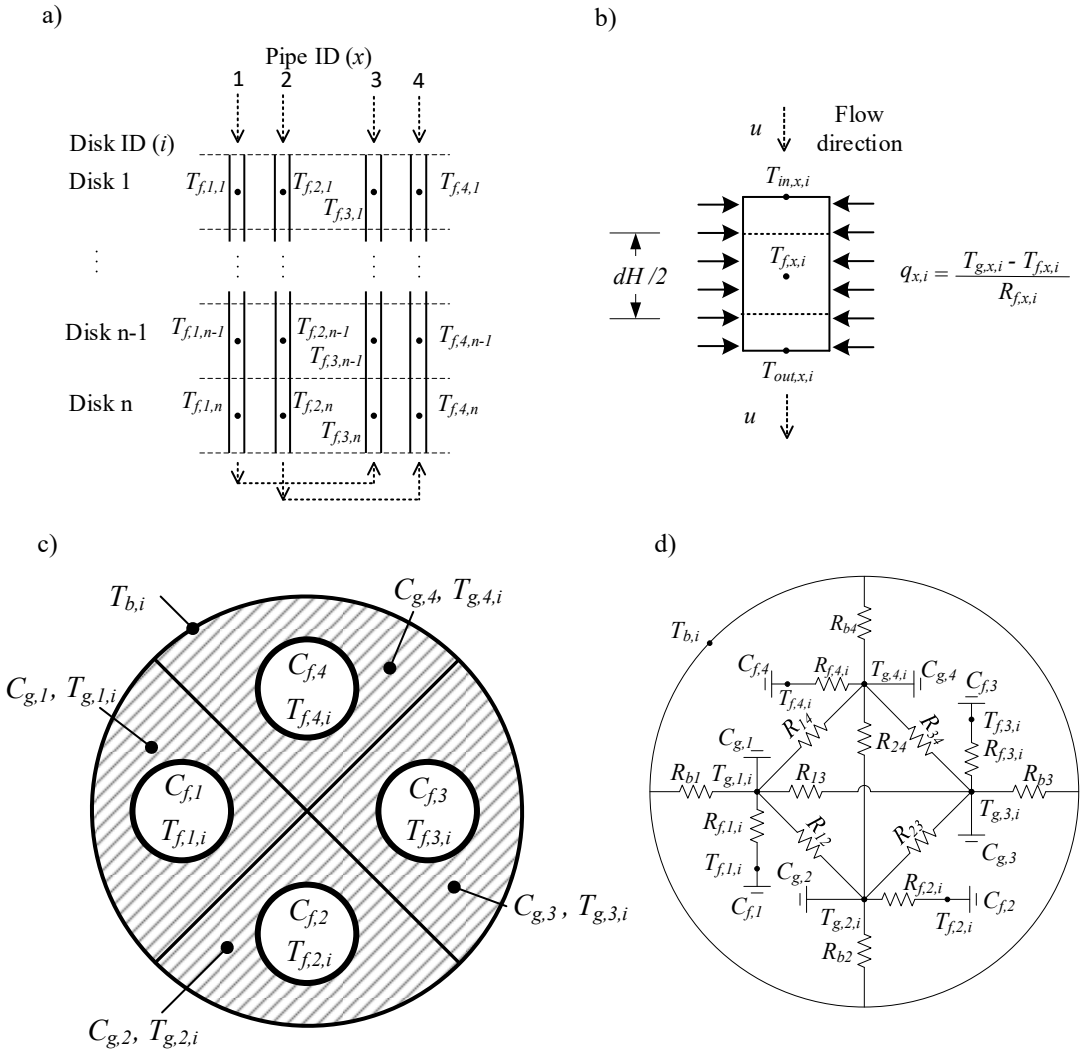

Figure 2 : Schematic of the TRC model: a) Nomenclature and vertical discretization; b) Control volume on fluid node for pipe $\boldsymbol{x}$ and disk $\boldsymbol{i}$; c) Cross-section showing the various capacitances; d) Thermal resistance network.

The so-called multipole method (Bennet et al., 1987) is used to evaluate all thermal resistances. This method takes into account the geometry of the borehole as well as the thermal properties of the grout and the ground. As shown in Figure 3, thermal resistance values depend on the order of the multipole but insignificant differences can be observed after the fifth order (Marcotte, 2016). Finally, for a symmetrical geometry, $R_{13} = R_{24}$, $R_{12} = R_{23} = R_{34} = R_{14}$, and $R_{b1} = R_{b2} = R_{b3} = R_{b4}$.

.

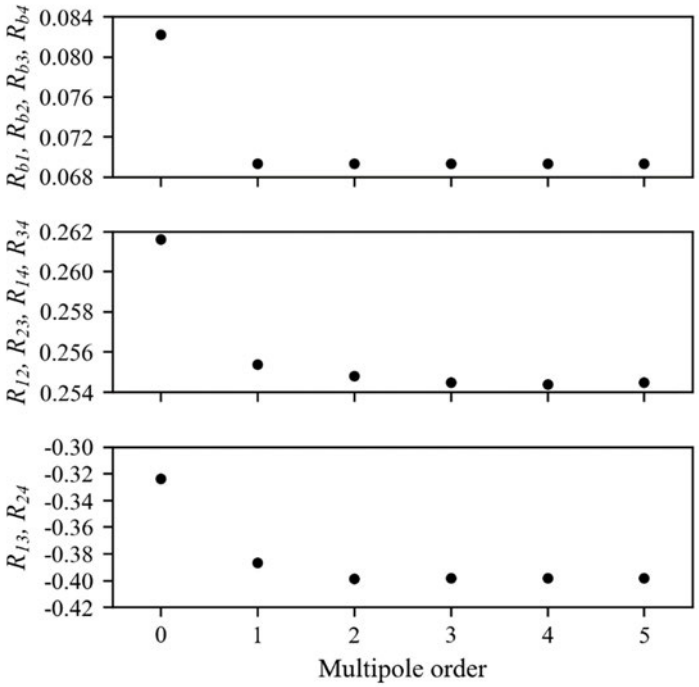

Figure 3 : Thermal resistance values for the geometry presented in Figure 2 and in Table 1

The thermal resistances identified as $R_{f,x,i}$ are the sum of the convection thermal resistance and pipe conduction thermal resistance. They are calculated as follows:

$$R_{f,x,i} = \frac{1}{2\,\pi r_i h_{x,i}} + \frac{1}{2\pi k_p} \ln\left(\frac{r_o}{r_i}\right) \tag{1}$$

where r_i and r_o are the pipe internal and external radius and k_p is the pipe thermal conductivity. For long boreholes, the axial dependency of the internal film coefficient, $h_{x,i}$, can be neglected and the i index can then be dropped. Thus, uniform film coefficients are assumed for each pipe. The value of h_x depends on the type of flow regime in the pipe. For laminar flow, h_x is evaluated based on a constant value of the Nusselt number (Nu=4.36). For turbulent flows down to transition-to-laminar conditions, the well-known

Gnielinski correlation is used (see Javed and Spitler (2016)). When there is no flow, the relation suggested by Wetter and Huber (1997) is used to compute h_x where k_f is the fluid thermal conductivity.

$$\boldsymbol{h_x = \frac{k_{f,x}}{r_p(1-\sqrt{0.5})}} \tag{2}$$

These relationships to determine h_x are typically used for long boreholes. For short boreholes such as the one used in the present experimental study, the thermal entry length has to be considered and ideally the axial dependency of the internal film coefficient should be accounted.

The thermal capacity of the grout and of the heat carrier fluid are identified by $C_{g,x}$ and $C_{f,x}$, respectively. As indicated in Equation 3, each of the $C_{g,x}$ value is equal to one quarter of the total grout thermal capacity.

$$C_{f,x} = \rho_{f,x} Cp_{f,x} \pi r_p^2, \qquad C_{g,x} = \frac{C_{gt}(\pi r_b^2 - 4\pi r_o^2)}{4} \tag{3}$$

where $\rho_{f,x}$ and $Cp_{f,x}$ are the density and specific heat of the fluid in pipe x, C_{gt} is the grout volumetric heat capacity (kJ m^{-3} K^{-1}), and r_b is the borehole radius The thermal capacity of the pipes is neglected because of its relatively small influence on the transient response of boreholes as shown by Shirazi & Bernier (2013).

Following the approach of Godefroy (2014) and Al-Khoury (2011), the governing equations of the TRC network are presented below. The derivation of equations 4 and 6 is presented in the Appendix. In essence, since axial heat transfer is neglected, TRC models solve the governing heat transfer equations for each vertical disk to obtain temperature nodes, $T_{g,x,i}$ and $T_{b,i}$, respectively.

$$\sum_{j=1,j\neq x}^{4}\left[\frac{T_{g,j,i}-T_{g,x,i}}{R_{xj}}\right] + \frac{T_{b,i}-T_{g,x,i}}{R_{bx}} + \frac{T_{f,x,i}-T_{g,x,i}}{R_{f,x,i}} = \frac{C_{g,x}}{\Delta t}\left(T_{g,x,i} - T^0_{g,x,i}\right) \tag{4}$$

for $x = 1$ to 4 and $i = 1$ to n

$$\sum_{j=1}^{4} \frac{T_{g,j,i} - T_{b,i}}{R_{bj}} = Q_{b,i} \qquad \text{for } i = 1 \text{ to } n \tag{5}$$

where Δt is the time step, $T^0_{g,x,i}$ is the grout temperature around pipe x in disk i at the previous time step, and $Q_{b,i}$ is the total heat transfer rate per unit length for disk i.

With reference to Figure 2b and as shown in the appendix, the fluid temperature in pipe x and disk i is given by:

$$\frac{\dot{m}_x c_{p_{f,x}}}{dH}\left(T_{in,x,i} - T_{out,x,i}\right) - \frac{(T_{f,x,i} - T_{g,x,i})}{R_{f,x,i}} = \frac{C_{f,x}}{\Delta t}\left(T_{f,x,i} - T^0_{f,x,i}\right) \quad \text{for } x = 1 \text{ to } 4 \text{ and } i = 1 \text{ to } n \tag{6}$$

$$T_{in,x,i} = T_{out,x,m} \quad \text{where } m = i - 1 \text{ (downward flow) or } i + 1 \text{ (upward flow)} \tag{7}$$

$$T_{f,x,i} = \frac{T_{in,x,i} + T_{out,x,i}}{2} \quad \text{for } x = 1 \text{ to } 4 \tag{8}$$

The borehole wall temperature of each disk at time t_n is evaluated using a ground thermal response factor based on the analytical cylindrical heat source solution as follows:

$$T_{b,i}(t_n) = T_{g,init} + \Delta T^*_i(t_n) + Q_{b,i}(t_n)\frac{G(Fo_{(t_n - t_{n-1})})}{k_s} \tag{9}$$

where $T_{g,init}$ is the initial ground temperature, $Q_{b,i}(t_n)$ is the heat transfer rate per unit length for vertical section i at the current time step, and G is the ground thermal response factor for a given Fourier number ($Fo = \alpha t / r_b^2$). ΔT^*_i is the ground temperature variation at the borehole wall computed by superposing known values of $Q_{b,i}$ at previous time steps (Godefroy, 2014):

$$\Delta T_i{}^*(t_n) = \sum_{i=1}^{n-1} \left[Q_{b,i}(t_i) - Q_{b,i}(t_{i-1})\right]\frac{G(Fo_{(t_n - t_{i-1})})}{k_s} - Q_{b,i}(t_{n-1})\,\frac{G(Fo_{(t_n - t_{n-1})})}{k_s} \tag{10}$$

Values of G are evaluated using the approximation proposed by Cooper (1976).

For each vertical disk there are 18 unknowns, i.e. 17 temperatures ($T_{f,x,i}$, $T_{in,x,i}$, $T_{out,x,i}$, and $T_{g,x,i}$, for i=1 to 4, and $T_{b,i}$) and $Q_{b,i}$ and 18 governing equations (Equations 4 to 9). Therefore, the proposed model solves a system of $18n$ unknowns combined with $18n$ linear equations at each simulation time step for a borehole discretized with n vertical disk. A total of 10 vertical sections are used for the tests reported in this paper based on a grid independent study. A time step of 1 s is used in the model to match the data acquisition frequency. The model inputs are the inlet temperatures and fluid flow rates in pipes #1 and #3.

Before undertaking an experimental validation of the TRC model, the single U-tube version of the TRC model presented above was verified against the step change test provided by Rees and He (2013). The results of this verification (Godefroy and Bernier, 2014) showed that the TRC model was giving good results and that the governing equations were correctly implemented.

4. Experimental set-up

The experimental set-up consists of a small-scale double U-tube borehole and a tank filled with laboratory-grade sand. These components are shown in Figure 4 and a cross-section of the borehole is presented in Figure 5. The main characteristics of the borehole and of the sand tank are summarised in Table 1. In addition, the U-tubes are fed by two independent water supply circuits and a data acquisition system is used to acquire and store measured data (Marcotte, 2016).

The active section of the borehole is 90.39 cm long and has a diameter of 9.45 cm. The top of the borehole is positioned 4 cm beneath the sand surface. As shown in Figure 5, the borehole contains four pipes arranged in two circuits with a 1-3, 2-4 configuration (see Figure 1). A solid ceramic (www.aremco.com) compound is used as grout. This is done for two main reasons. First, thermal properties are more likely to be homogenous than a regular grout mix and secondly, the ceramic can easily be machined to introduce pipes and temperature sensors at precise locations. The thermal properties of the ceramic were measured using the transient plane heat source method in accordance with ISO22007-2.2 with resulting values of thermal conductivity and thermal capacity of 4.45 $Wm^{-1}K^{-1}$ and 2500 kJ m^{-3} K^{-1}, respectively.

As shown in Figure 5, four symmetrically located holes are machined in the ceramic. Stainless steel pipes with an external diameter of 1.905 cm and a thickness of 0.1651 cm are inserted into the ceramic holes and held in place with a small layer of glue so as to avoid air gaps. At the bottom of the borehole (Figure

4 bottom left), a machined block of plastic connects each opposite stainless steel pipe to form the 180° turn of each U-tube.

As indicated on the left portion of Figure 4, there are temperature measurements at the inlet and outlet of the four pipes (only two pipes are shown) and at the bottom of each of the four pipes. These fluid temperatures are measured using RTDs with an uncertainty of ±0.15 °C. Specially fabricated mixers are positioned upstream of these RTD to ensure accurate average temperature measurements. At mid-height, twenty-nine thermocouples are positioned as follows (see Figure 5): sixteen are fixed along the periphery of the ceramic cylinder to measure borehole wall temperature: eight are inserted evenly along a 8.04 cm diameter circle; four are situated evenly along a 4.72 cm diameter circle which coincides with the center of the stainless-steel pipes; and the last one is inserted at the geometric center.

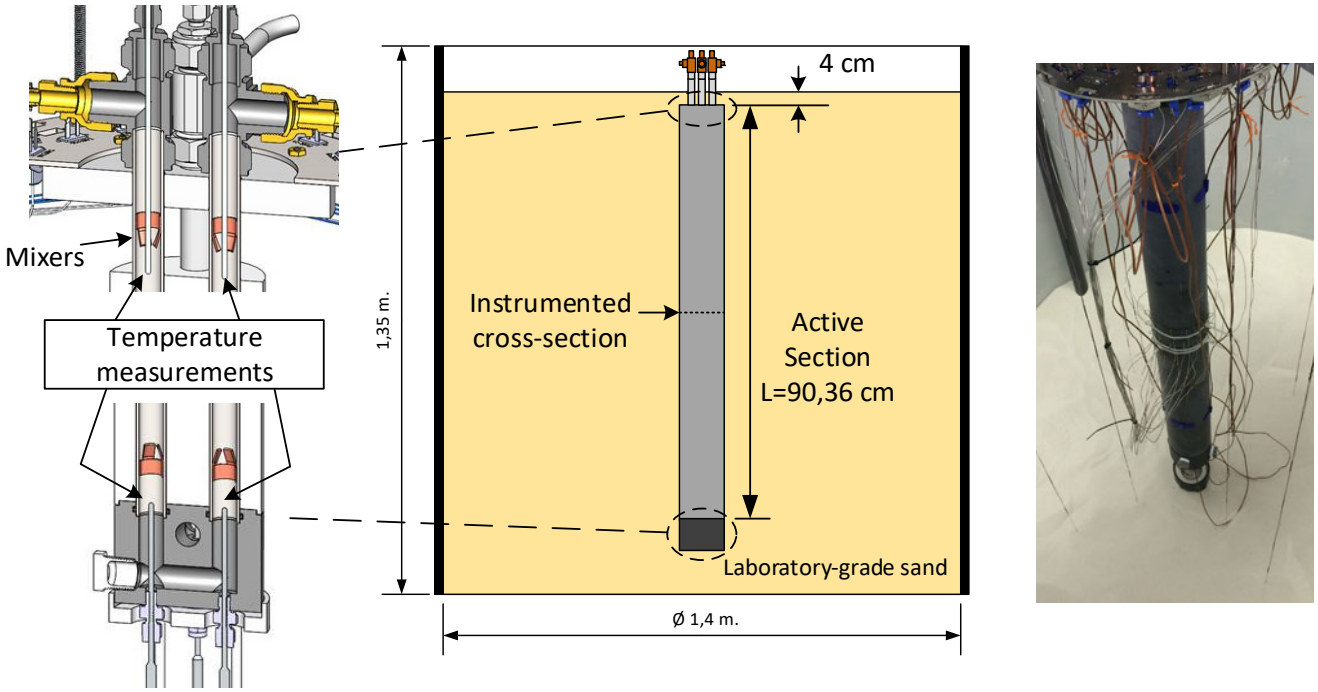

Figure 4: Double U-tube borehole used in the present study: Inlet an outlet temperature measurements (top-left); Bottom temperature measurements in the 180° bend (bottom-left); Position of the borehole in the sand tank (center); Instrumented borehole in the partially-filled sand tank (right).

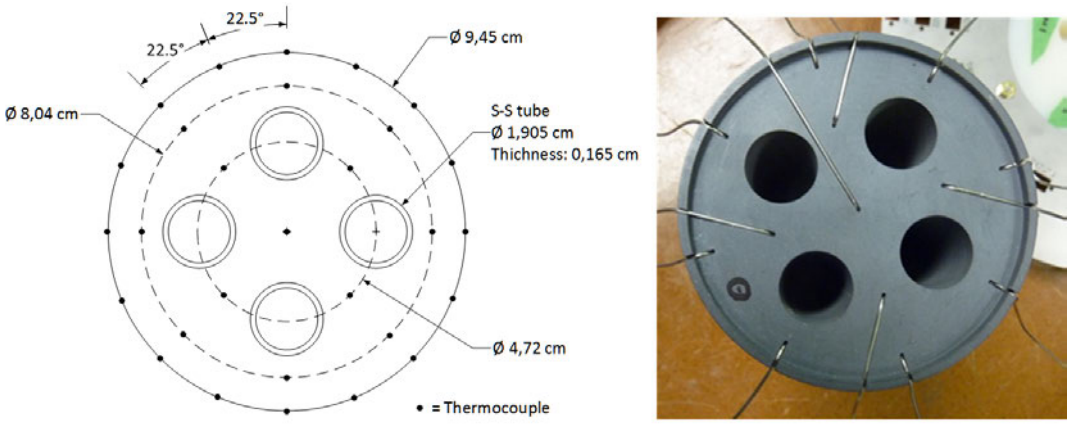

Figure 5: Cross-section at the mid-height of the borehole showing thermocouple locations.

Epoxy glue is used to fix these thermocouples. All thermocouples in the borehole were calibrated with a resulting uncertainty of ±0.25 °C. Thermocouples installed in the sand tank have an uncertainty of ±0.35 °C (Salim Shirazi & Bernier, 2014).

Table 1: Experimental set-up characteristics

	Parameter	Value	Units
Borehole	Height	90.39	cm
	Diameter	9.45	cm
	Pipe external diameter	1.905	cm
	Pipe thickness	0.1651	cm
	Pipe thermal conductivity	16.2	$Wm^{-1}K^{-1}$
	Grout thermal conductivity	4.45	$Wm^{-1}K^{-1}$
	Grout volumetric heat capacity	2500	$kJm^{-3}\ K^{-1}$
Sand tank	Height	1.35	m
	Diameter	1.40	m
	Sand thermal conductivity	0.29	$Wm^{-1}K^{-1}$
	Sand thermal diffusivity	0.0198	m^2/day

As shown on the photo in Figure 4, the borehole is positioned vertically in the center of a sand tank. The tank has a height of 1.35 m and a diameter of 1.40 m and is filled with so-called Ottawa sand. The thermal properties of this laboratory grade sand were studied by Tarnawski et al. (2009) and are reported in Table

1. Thermocouples are fixed with fishing wire into the sand tank to measure sand temperatures at specific depths and radius (Salim Shirazi and Bernier (2014). Constant temperature boundary conditions, corresponding to the lab temperature, are assumed on all sides of the tank.

The heat carrier fluid is tap water. Each U-tube is connected to an independent pumping circuit. For each of these circuits, the circulating fluid temperature is precisely maintained using a thermostatic bath and the flow rate is controlled by a needle valve. The flow rate in each circuit is measured by high precision turbine flow meters. Each flow meter was calibrated to a relative uncertainty of ±1.7 %. A standard Labview-based data acquisition system is used and all measurements are recorded at a high frequency (every second) to capture transient effects.

As shown by Marcotte (2016), a typical test starts by recirculating the fluid in the circuit without routing it to the borehole which allows the flow rates to be adjusted to the targeted values. Once the desired fluid temperature is reached, the fluid is directed to the borehole. Temperatures and flow rates can be varied during a test from 10 °C to 80 °C and from 200 ml/min to 900 ml/min, respectively. For one of the tests reported in the results section, flow meters are bypassed to achieve higher flow rates (4 L/min) to minimize the inlet/outlet temperature difference. For this test, the flow rate is evaluated by measuring the mass of water accumulating in a bucket over time. Finally, the residence time of the fluid is approximatey 30 s when the flow rate is 750 ml/min.

The thermal resistance values and node thermal capacities for the present experimental borehole geometry are given in Table 2. As indicated earlier, the thermal resistances are obtained using the multipole method.

Table 2 : Thermal resistances and node thermal capacities for the present borehole geometry.

Parameter	Value	Units
$R_{12}, R_{23}, R_{14}, R_{34}$	0.2545	m-K/W
R_{13}, R_{24}	-0.3983	m-K/W
$R_{b1}, R_{b2}, R_{b3}, R_{b4}$	0.0693	m-K/W
$C_{g,x}$	3.67	kJ/m-K
$C_{f,x}$	0.818	kJ/m-K

5. Results

A total of three sets of experimental results are reported. The first experiment uses measured temperatures at the mid-height cross-section to draw isotherms for comparison with the multipole method. The second and third experiments are used to determine if the proposed TRC model can reproduce the measured outlet temperatures when the borehole is in transient state.

5.1 Isotherms at the mid-height cross-section

In this experiment, the two circuits are fed with constant inlet fluid temperatures of 17 °C and 27 °C, respectively. The flow rate is set at 4 L/min in each circuit resulting in a ≈ 0.2 K temperature difference between the inlet and outlet of each circuit. The multipole method computes heat transfer in the borehole for steady-state conditions. Given that ground heat transfer is always in transient state, it is not possible to reach a pure steady-state condition. However, based on the time evolution of the twenty-nine temperature measurements at the mid-height cross-section shown in Figure 6, it was determined that a quasi-steady-state was reached after 36 minutes.

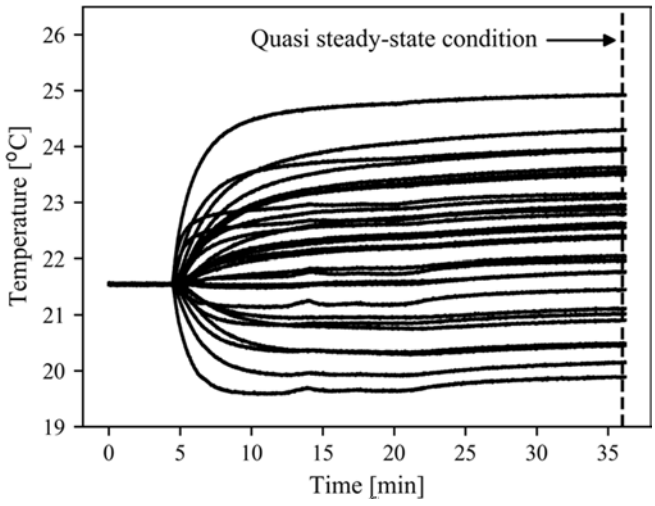

Figure 6: Evolution of the twenty-nine temperature measurements (see position in Figure 5) at the mid-height cross-section for the isotherm test.

Temperatures at the mid-height cross-section are then recorded and isotherms are drawn as shown in Figure 7. The measured temperatures are presented on the left. The experimental isotherms (center) are generated using a cubic interpolation of the measured temperatures inside the grout combined with the water fluid temperature at the borehole mid-height which is estimated based on a linear temperature

variation from the inlet to outlet. It is to be noted that one thermocouple (shown by a dark circle on the left) failed during the experiments and could not be used to determine the isotherms. The isotherms, evaluated with the multipole method are based on the thermal resistances presented in Table 2, are shown on the right in Figure 7.

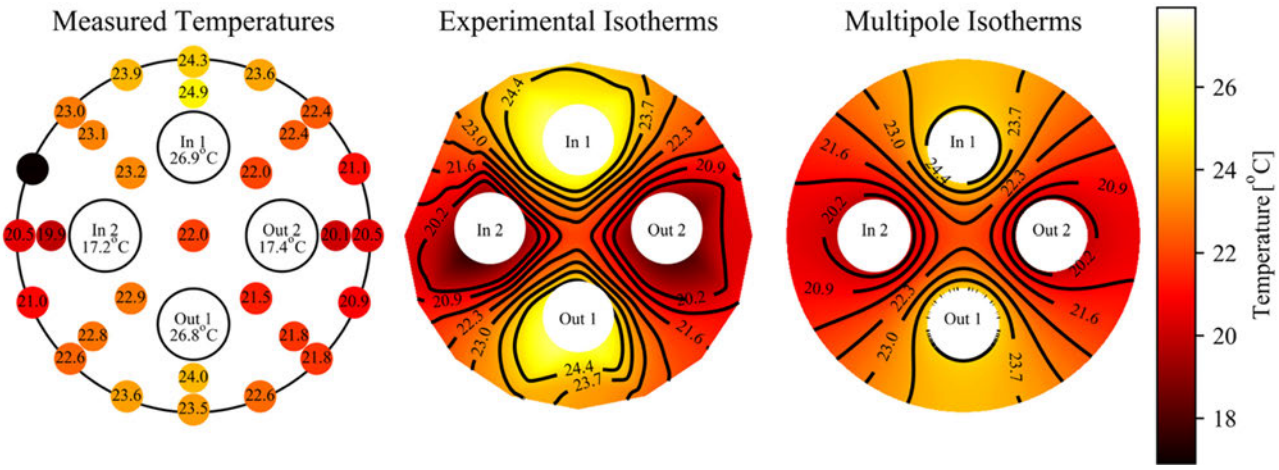

Figure 7: Comparison between measured and calculated isotherms at mid-height.

The agreement between the isotherms generated with the experimental data and the ones obtained with the multipole method is very good. Some discrepancies can be seen around the pipes. These can be attributed to the use of a discrete temperature point to represent the water fluid temperature in the pipe cross-section.

5.2 Step change in inlet conditions

In this test, each circuit is subjected to a step change in inlet temperatures. As shown in Figure 8, the tank temperature is stable at 22.0 °C for the first 22 minutes. During that period, water from the temperature baths is recirculated to stabilize flow rates and temperatures in the two independent water supply circuits. Then, at t = 22 min, tubes #1 and #2 are fed with water from these supply circuits at a constant inlet temperature of 48.4 °C and with a nominal flow rate of 750 ml/min. Thus, both circuit experience a temperature step change of 26.4 °C over a period of approximately 3 min.

The top graph in Figure 8 shows the variation of the experimental flow rate to both circuits for the duration of the test. The middle graph shows the time evolution of the experimental inlet temperatures to both

circuits. These sets of experimental data (flow rate and inlet temperatures), taken at 1 s intervals, are used as inlet conditions for the TRC model along with the measured initial ground temperature of 22.0 °C.

The bottom graph in Figure 8 shows a comparison between the measured and simulated outlet temperature for both circuits. For t > 100 min, the agreement between measured and simulated results is excellent and as shown in one of the insert, results from the model are within the experimental uncertainty for circuit 1-3 (similar results are obtained with circuit 2-4). However, near the step change in temperature at the beginning of the test, the TRC model tends to under predict the measured outlet temperatures. The maximum differences between the measured and simulated outlet temperatures are 3.68 °C and 3.47 °C for circuit 1-3 and 2-4, respectively. The TRC model relies on four grout nodes in the borehole each covering one quarter of the cross-section. This might not be sufficient to capture transient effects for rapidly changing conditions. These differences decrease rapidly to ≈ 0.5 °C, six minutes after the step change (i.e. at $t = 28$ min). Thus, it appears that the four-node configuration is a good compromise between ease-of-use and accuracy. It is to be noted that a real size typical borehole will have a residence time about 5 times higher than the one experienced here with this small-scale borehole. Furthermore, ground thermal properties in the field might be different. Thus, the TRC model may react differently for typical borehole conditions. However, Godefroy et al. (2016) have shown, for a single U-tube borehole that simulation results obtained using a TRC approach similar to the one presented here were in very good agreement with experimental results on a 76 m long borehole.

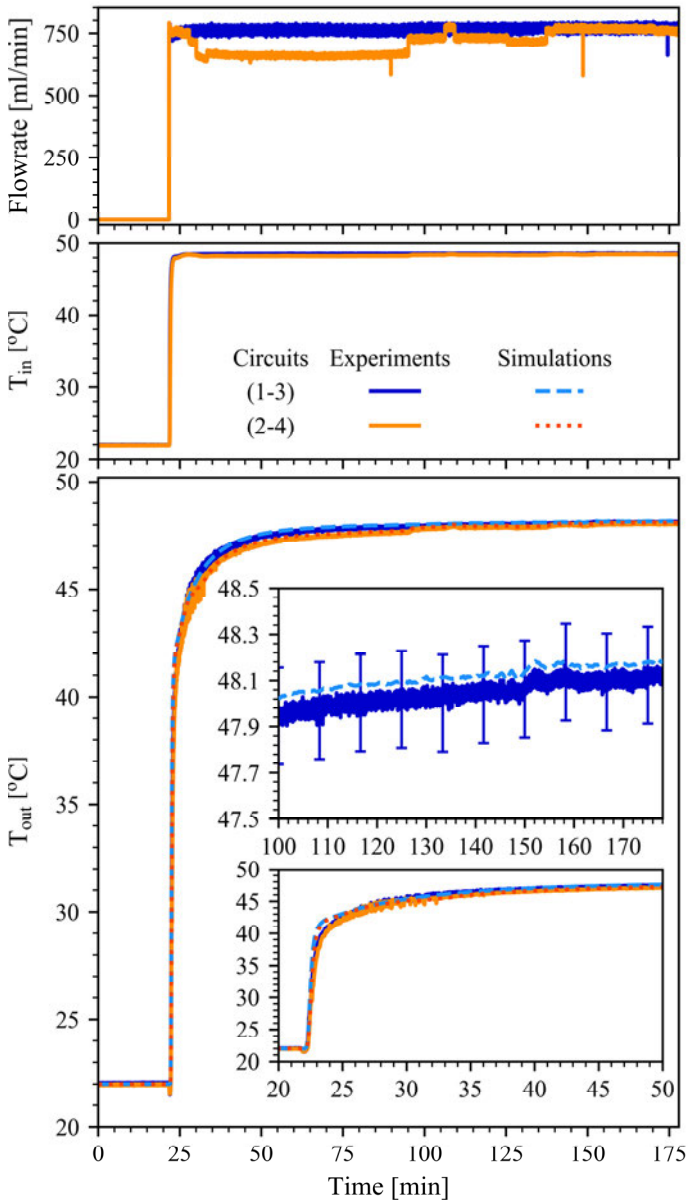

Figure 8: Results for constant inlet conditions

5.3 Variable inlet conditions

The third test is performed for variable inlet conditions to both circuits. These conditions are shown on the top two graphs in Figure 9. The data acquisition system is initiated at $t = 0$. There is no flow until $t = 1$ min and all temperatures are equal to the initial sand tank temperature (22.6 °C). Water is pumped in circuit 1-3 starting at $t = 1$ min at a nominal flow rate of 750 ml/min. The inlet temperature reaches a

constant nominal value of 38.8 °C at $t = 3$ min. These conditions are held constant until $t = 39$ min. Then, water pumping in circuit 1-3 is stopped and the flow rate in that circuit remains at zero until $t = 62$ min. Then, the water pump for circuit 1-3 is restarted with a flow rate of 650 ml/min which gradually decreases down to 590 ml/min at the end of the test at $t = 160$ min. Starting at $t = 62$ min, the inlet temperature in circuit 1-3 experiences a sudden increase up to 48 °C. Then, at $t = 102$ min, the inlet temperature is gradually decreased down to 30 °C over a period of 24 min. Finally, the inlet temperature remains at that value for the remainder of the test.

The scenario is different for circuit 2-4. The flow rate is fixed at 750 ml/min for the first 80 min. Then, the flow is stopped from $t = 80$ min to $t = 101$ min. The pump is reactivated for $t > 101$ min and the nominal flow rate is 725 ml/min until the end of the test. The inlet temperature is held constant at ≈39 °C for the first 80 min. Then, when the flow is reactivated at $t >$101 min, the inlet temperature is set at 32 °C and it decreases gradually down to 20 °C over the next 20 min and it remains at that temperature for the rest of the test. These values of flow rate and inlet fluid temperatures are used as inputs to test the TRC model for rapidly changing conditions.

The bottom graph in Figure 9 shows a comparison between the experimental results and the output of the TRC model. Results for circuit 1-3 are examined first. Results for the first 40 minutes when the inlet conditions are constant are similar to the results presented in Figure 8. The maximum differences in the outlet temperatures between the results of the TRC model and the experimental data is 1.9 °C. When there is no flow in circuit 1-3, i.e. when $39 < t < 62$ min, the TRC model fails to correctly predict the measured outlet temperature. The TRC model predicts an outlet temperature, i.e. the temperature in the outlet disk, lower than the one measured over the interval $39 < t < 46$ min. However, for $46 < t < 62$ min, the outlet temperature predicted by the TRC model is higher than the measured value. This difference is about 1.5 °C at $t = 62$ min. The exact source of this discrepancy is unknown. It is speculated that the natural convection heat transfer coefficient used in cases when there is no flow (Eq. 2) might be inadequate for the current geometry. The determination of natural convection heat transfer coefficients in boreholes is outside the scope of the present analysis. However, a sensitivity analysis is performed on the value of the heat transfer coefficient when there is no flow. For the purpose of this analysis, the value of the heat transfer coefficient calculated with Eq.2 is multiplied by 100 and 0.1, respectively. As shown in Figure 10 for $39 < t < 46$ min, the heat transfer coefficient that would minimize the difference between the experimental and modeling results is probably between h (calculated with Eq. 2) and $0.1h$.

However, for t > 46 min, even a heat transfer coefficient 100 times higher that the one predicted by Eq.2, is unable to predict the experimental temperature drop. Another possible cause of the discrepancy is the fact that the measured outlet temperature might be affected by surface effects as the outlet temperature is measured 4 cm below the sand-air interface.

If the TRC model is used in a simulation, the inability to predict the correct outlet temperature for a no flow condition has no consequence as the borehole is not used. What is reassuring is that as soon as flow is reactivated in the borehole, the TRC model results are in good agreement with the experimental data. Hence, for $t > 62$ min, when the flow rate is non-zero, the agreement between the experimental results and the TRC model is very good with a root mean square difference of 0.2 °C.

The experimental results and the TRC model are in very good agreement for the first 80 minutes for circuit 2-4. During that period the maximum difference is 1.2 °C and the root mean square error is 0.15 °C. For $62 < t < 80$ min, the TRC model is able to capture the small temperature increase caused by the temperature increase in circuit 1-3. When the flow rate is stopped in circuit 2-4 ($80 < t < 100$ min), the TRC model is unable to correctly predict the outlet temperature. A maximum difference of 2.5 °C can be observed at t = 101 min. Here again, it is speculated that the heat transfer coefficient might be inaccurate or the outlet temperature might be affected by the sand-air interface. However, when the flow is re-established in circuit 2-4 at $t > 100$ min, the agreement between the experimental data and the TRC model is very good with a maximum difference of 0.5 °C.

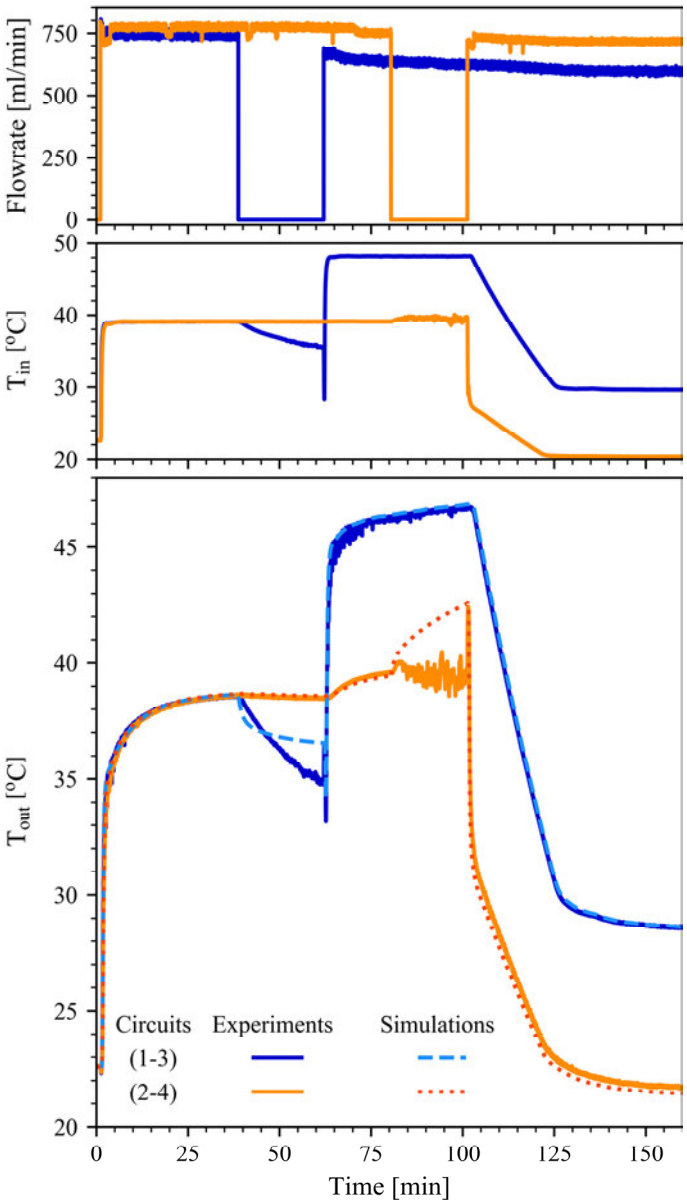

Figure 9: Results for variable inlet conditions.

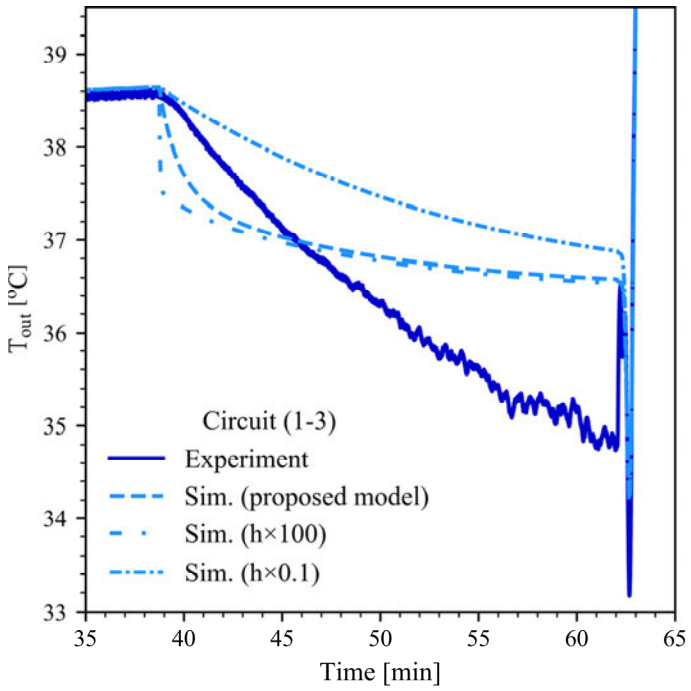

Figure 10: Sensitivity analysis on the value of the natural convection heat transfer coefficient.

6. Conclusion

A thermal resistance and capacitance (TRC) model of a double U-tube borehole with two independent circuits is presented in this paper. Results from the model are compared with experimental data obtained on a small-scale borehole positioned in a tank filled with laboratory-grade sand.

Contrary to other TRC models, the proposed model is restricted to the borehole itself while heat transfer from the borehole wall to the far field is calculated with the infinite cylindrical heat source solution with proper temporal superposition to handle the thermal history. The borehole is subdivided into n vertical disks each of which are composed of four quadrants with corresponding fluid and grout temperatures. A series of thermal resistances and capacitances (see figure 2) link the four grout temperatures and the borehole wall temperature of each disk. A fifth order multipole is used to compute tube-to-tube and tube-to-borehole wall thermal resistances.

The small-scale borehole is 90.39 cm long with a diameter of 9.45 cm. It is equipped with RTD sensors that measure inlet and outlet temperatures. Furthermore, twenty-nine thermocouples measure the mid-height cross-section temperatures. Two temperature baths are used to supply water at two different temperatures and flow rate for both circuits. Data are recorded at 1 s intervals to properly capture transient effects.

A first set of results shows that the cross-section isotherms measured experimentally compare favourably well with the ones calculated using the multipole method. In the second test, a step change of 26.4 °C in the inlet temperature is imposed in both circuits. It is shown that the TRC model results are in very good agreement with the experimental data except for a few minutes immediately after the step change where there is a discrepancy of ~ 3.5 °C. This difference diminishes rapidly and TRC model results are eventually within the experimental uncertainty. In the third test, both circuits experience significant variations (temperature and flow rate) of inlet conditions, including episodes of no flow. Here again, the agreement between the prediction of the outlet temperature by the TRC model and the experimental data can be considered to be very good except when there is no flow where the model fails to reproduce adequately the outlet temperature.

More work is needed to develop better convection coefficient correlations for natural convection cases when there is no flow in boreholes which might improve the results of the TRC model in such cases.

Nonetheless, the four-node TRC model presented in this paper is a good compromise between ease-of-use and accuracy.

Acknowledgements

The financial support provided by the Natural Science and Engineering Research Council of Canada through a discovery grant and NSERC's Smart Net-Zero Energy Buildings Strategic Research Network is gratefully acknowledged.

Nomenclature

A : Cross-sectional flow area [m^2]

$C_{f,x}$: Fluid thermal capacity in pipe x [J m^{-1} K^{-1}]

$C_{g,x}$: Grout thermal capacity for the quadrant of pipe x [J m^{-1} K^{-1}]

C_{gt} : Grout volumetric heat capacity [J m^{-3} K^{-1}]

$Cp_{f,x}$: Specific heat of the fluid in pipe x [J kg^{-1} K^{-1}]

dH : Height of each vertical disk [m]

Fo : Fourier number [-]

h_x: internal film coefficient for pipe x [W m^{-2} K^{-1}]]

i: Identification of the vertical disks

$k_{f,x}$: Thermal conductivity of the fluid in pipe x [W m^{-1} K^{-1}]

k_s : Thermal conductivity of the ground [W m^{-1} K^{-1}]

$\dot{m}$: Mass flow rate [kg/s]

$Q_{b,i}$: Total heat transfer rate per unit length for disk i [W m^{-1}]

r_b : Borehole radius [m]

r_o: Outer radius of U-tubes [m]

r_p: Inlet radius of U-tubes [m]

R: Resistances in the thermal network illustrated in Figure 2

t_n : Time at the timestep n [s]

$T_{b,i}$: Borehole wall temperature for disk i [C]

$T_{f,x,i}$ **:** Fluid temperature for disk i pipe x [C]

$T_{g,x,i}$: Grout temperature around pipe x in disk i [C]

$T_{g,init}$: Initial ground temperature [C]

$T_{in,x,i}$: Temperature entering the vertical disk i in pipe x [C]

$T_{out,x,i}$: Temperature exiting the vertical disk i in pipe x [C]

u : Fluid velocity [m/s]

x: Pipe identification (1, 2, 3 or 4)

Greek letters

α : Thermal diffusivity of the ground [m^2/s]

ϕ : Dependent variable (= $C_p T$)

$\rho_{f,x}$: Density of the fluid in pipe x [kg/m^3]

Δt : Value of the timestep [s]

ΔT_i^* : Ground temperature variation at the borehole wall in Eq. (9)

Superscript:

^{0}: Indicate an element at the previous time step

Appendix

Equations 4 and 6 presented in the text are derived in this appendix.

With reference to Figure 2c, the calculation domain is assumed to be composed of a cylinder with four quadrants, each represented by one grout node. Each quadrant has an internal convection boundary condition with the circulation fluid at T_f and conduction with the borehole wall at T_b. Assuming constant properties and negligible axial conduction, the governing unsteady heat equation in polar coordinates for the solid portion of the borehole is given by:

$$\rho C_p \frac{\partial T}{\partial t} = \frac{1}{r}\frac{\partial}{\partial r}\left(rk\frac{\partial T}{\partial r}\right) + \frac{1}{r}\frac{\partial}{\partial \theta}\left(\frac{k}{r}\frac{\partial T}{\partial \theta}\right) \tag{A-1}$$

Following the finite volume approach of Patankar (1980) and using the fully implicit scheme (the new value of T_P prevails over the entire time step), the discretized equation for a grout node P surrounded by three grout nodes (E, W, S) and the borehole wall node (N) is derived by integrating over the control volume (ΔV) and over the time interval from t to $t + \Delta t$:

$$a_P T_P = a_E T_E + a_W T_W + a_N T_N + a_S T_S + b \tag{A-2}$$

where

$$a_E = \frac{k_e \Delta r}{r_e (\delta\theta)_e}\,, a_W = \frac{k_w \Delta r}{r_w (\delta\theta)_w}\,, a_N = \frac{k_n r_n \Delta\theta}{(\delta r)_n}, a_S = \frac{k_s r_s \Delta\theta}{(\delta r)_s}, b = a_P^0 T_P^0 + hT_f$$

$$a_P = a_E + a_W + a_N + a_S + a_P^0 + h \quad with \quad a_P^0 = \frac{\rho C_p \Delta V}{\Delta t} \text{ and } h = 1/R_f \tag{A-3}$$

Values of a_E, a_W, a_N, a_S are thermal conductances (inverse of thermal resistances) between the various nodes and T_P^0 is the grout node temperature at the previous time step. The thermal resistances are calculated using the multipole method and are presented in Figure 3. The internal convection boundary condition is included in the b and a_P terms as suggested by Patankar (1980) where the value of R_f is

defined in Equation 1. As an example, the discretized equation for ground node $T_{g,1}$, for one vertical segment i, is given by :

$$\left(\frac{1}{R_{12}}+\frac{1}{R_{14}}+\frac{1}{R_{b1}}+\frac{1}{R_{13}}+\frac{\rho C_p \Delta V}{\Delta t}+\frac{1}{R_f}\right)T_{g,1}=\frac{1}{R_{12}}T_{g,2}+\frac{1}{R_{14}}T_{g,4}+\frac{1}{R_{b1}}T_b+\frac{1}{R_{13}}T_{g,3}+\frac{\rho C_p \Delta V}{\Delta t}T_{g,1}^0+\frac{1}{R_f}T_{f,1} \qquad \text{(A-4)}$$

where ($V=(\pi r_b^2-4\pi r_o^2)/4$). Similar equations are obtained for $T_{g,2}$, $T_{g,3}$, and $T_{g,4}$ and rearranged in a compact form to obtain Equation 4 for all segments i.

As shown in Figure 2b, the fluid control volume is subjected to a heat flux boundary condition (q) at the periphery. Assuming no axial heat conduction in the fluid, the governing equation for an unsteady one-dimensional convection-diffusion situation is given by:

$$\frac{\partial(\rho\phi)}{\partial t}+\frac{\partial(\rho u\phi)}{\partial x}=0 \qquad \text{(A-5)}$$

where $\phi=C_pT$ and u is the fluid velocity. Assuming equidistant nodes and using the fully implicit scheme for time and a central difference scheme, the discretized equation for a fluid node P with upstream and downstream nodes W, E is derived by integrating over the control volume ($dH/2$) and over the time interval from t to $+\Delta t$ (Patankar, 1980).

$$a_PT_P=a_WT_W+a_ET_E+b \qquad \text{(A-6)}$$

where

$$a_E=-\frac{\rho uC_p}{2}\,,a_W=\frac{\rho uC_p}{2}\,,a_P^0=\frac{\frac{\rho C_p dH}{2}}{\Delta t},b=a_P^0T_P^0+q/2\,,\text{and}\;\; a_P=a_P^0 \qquad \text{(A-7)}$$

With reference to the nomenclature presented in figure 2b, Equation A-6 can be written as:

$$\frac{\rho C_p dH/2}{\Delta t}\left(T_{f,x,i} - T^0_{f,x,i}\right) = \frac{\rho u C_p}{2} T_{in,x,i} - \frac{\rho u C_p}{2} T_{out,x,i} + \frac{T_{g,x,i} - T_{f,x,i}}{2\, R_{f,x,i}} \qquad \text{(A-8)}$$

with $u = \dot{m}/\rho A$ (with $A = \pi r_p^2$), Equation A-8 leads to Equation 6.

References

Abdelaziz, S. T, & Ozudorgu, T.Y. (2016). Selection of the design temperature change for energy piles. Applied thermal engineering, 3(4), 237-252, doi.org/10.1016/j.applthermaleng.2016.07.067.

Al-Khoury, R. 2011. Computational Modelling of Shallow Geothermal Systems. London, CRC press.

Bauer, D., Heidemann, W., Müller-Steinhagen, H., & Diersch, H. J. (2011). Thermal resistance and capacity models for borehole heat exchangers. International Journal of Energy Research, 35(4), 312-320. https://doi.org/10.1002/er.1689.

Beier, R. A., Smith, M. D., & Spitler, J. D. (2011). Reference data sets for vertical borehole ground heat exchanger models and thermal response test analysis. Geothermics, 40(1), 79-85. https://doi.org/10.1016/j.geothermics.2010.12.007.

Bennet, J., Claesson, J., & Hellström, G. (1987). Multipole method to compute the conductive heat flows to and between pipes in a composite cylinder. Notes on heat transfer 3. University of Lund.

Bergman, T. L., Incropera, F. P., & Lavine, A. S. (2011). Fundamentals of heat and mass transfer: John Wiley & Sons.

Brischoux, P., & Bernier, M. (2016). Coupling PV/T Collectors with a Ground-Source Heat Pump System in a Double U-tube Borehole. ASHRAE Winter Conference, Orlando, Florida. January 2016. Paper OR-16-C046.

Chapuis, S. (2009). Stockage thermique saisonnier dans un champ de puits géothermiques verticaux en boucle fermée. M.A.Sc. Thesis, École Polytechnique de Montréal, http://search.proquest.com/docview/751605537.

Claesson, J., & Javed, S. (2011). An analytical method to calculate borehole fluid temperatures for time-scales from minutes to decades. ASHRAE Transactions, 117(2), 279-288.

Claesson, J., & Javed, S. (2018). Explicit Multipole Formulas for Calculating Thermal Resistance of Single U-Tube Ground Heat Exchangers. Energies, 11(1), 214. doi:10.3390/en1101021.

Cooper, L. Y. (1976). Heating of a cylindrical cavity. International Journal of Heat and Mass Transfer, 19(5), 575-577.

Cui, P., Yang, H., & Fang, Z. (2008). Numerical analysis and experimental validation of heat transfer in ground heat exchangers in alternative operation modes. Energy and Buildings, 40(6), 1060-1066. doi:10.1016/j.enbuild.2007.10.005

De Rosa, Ruiz-Calvo, F., Corberán, J., Montagud, C., & Tagliafico, L. (2014). Borehole modelling: a comparison between a steady-state model and a novel dynamic model in a real ON/OFF GSHP operation. Journal of Physics: Conference Series, Volume 547, (2014), https://doi.org/10.1088/1742-6596/547/1/012008.

De Rosa, M., Ruiz-Calvo, F., Corberán, J. M., Montagud, C., & Tagliafico, L. A. (2015). A novel TRNSYS type for short-term borehole heat exchanger simulation: B2G model. Energy Conversion and Management, 100, 347-357. https://doi.org/10.1016/j.enconman.2015.05.021.

Eskilson, P. (1987). Thermal analysis of heat extraction boreholes. Ph.D. thesis, University of Lund.

Eslami-Nejad, P., & Bernier, M. (2011a). Coupling of geothermal heat pumps with thermal solar collectors using double U-tube boreholes with two independent circuits. Applied Thermal Engineering, 31(14-15), 3066-3077. doi:10.1016/j.applthermaleng.2011.05.040.

Eslami-Nejad, P., & Bernier, M. (2011b). Heat transfer in double U-tube boreholes with two independent circuits. Journal of Heat Transfer, 133(8), 082801. doi:10.1115/1.4003747.

Eslami-Nejad, P., & Bernier, M. (2012). Simulations of a new double U-tube borehole configuration with solar heat injection and ground freezing. Proceedings of eSim 2012, 257-268.

Gentry, J. E. (2007). Simulation and validation of hybrid ground source and water-loop heat pump systems. M.Sc. thesis, Oklahoma State University.

Godefroy, V. and M. Bernier. 2014. A simple model to account for thermal capacity in boreholes. Proceedings of the 11th IEA 2014 Heat Pump conference, Montreal (Quebec), Canada, Paper #P.4.8. https://tinyurl.com/trc-model.

Godefroy, V. (2014). Élaboration et validation d'une suite évolutive de modèles d'échangeurs géothermiques verticaux, M.A.Sc thesis, École Polytechnique de Montréal.

Godefroy, V., Lecomte, C., Bernier, M., Douglas, M., & Armstrong, M. (2016). Experimental Validation of a Thermal Resistance and Capacity Model for Geothermal Boreholes. ASHRAE winter conference, Orlando, Florida, January 2016. Paper OR-16-C047.

Hellström, G. (1991). Ground heat storage: thermal analyses of duct storage systems: Ph.D. thesis, University of Lund, Sweden.

Hellström. G. (1989). Duct Ground Heat Storage. Manual for Computer Code. Department of Mathematical Physics, University of Lund, Sweden.

He, M. (2012). Numerical modelling of geothermal borehole heat exchanger systems. Doctoral Thesis. DeMontfort University.

Hern, S. A. (2004). Design of an experimental facility for hybrid ground source heat pump systems, M.Sc. thesis, Oklahoma State University.

Javed, S., & Spitler, J. (2016). Calculation of borehole thermal resistance. In: Simon J. Rees, editor. Advances in ground-source heat pump systems. Woodhead Publishing; 2016. 63-95. http://dx.doi.org/10.1016/B978-0-08-100311-4.00003-0.

Javed, S., & Spitler, J. (2017). Accuracy of borehole thermal resistance calculation methods for grouted single U-tube ground heat exchangers. Applied Energy, 187, 790-806. http://dx.doi.org/10.1016/j.apenergy.2016.11.079.

Kerme, E.D, & Fung, A.S. (2020). Heat transfer simulation, analysis and performance study of single U-tube borehole heat exchanger, Renewable Energy, 45, 1430-1448. doi.org/10.1016/j.renene.2019.06.004.

Kramer. C.A., Ghasemi-Fare, O. and Basu, P (2015). Laboratory thermal performance tests on a model heat exchanger pile in sand, Geotechnical and Geological Engineering, 33, 253-271.

Lecomte, C., & M. Bernier. (2016). Modélisation et simulation de puits géothermiques en série pour stockage saisonnier. Proceedings of the eSim 2016 Building Performance Simulation Conference, May 3-6, McMaster University, Hamilton, Ontario, Canada, 265-276.

Marcotte, B. (2016). Étude du transfert thermique transitoire dans les puits géothermiques à quatre tuyaux. M.A.Sc. thesis, École Polytechnique de Montréal. https://publications.polymtl.ca/2185/

Minaei, A., & Maerefat, M. (2017). A new analytical model for short-term borehole heat exchanger based on thermal resistance capacity model. Energy and Buildings, 146, 233-242. https://doi.org/10.1016/j.enbuild.2017.04.064.

Pärisch, P., Mercker, O., Oberdorfer, P., Bertram, E., Tepe, R., & Rockendorf, G. (2015). Short-term experiments with borehole heat exchangers and model validation in TRNSYS. Renewable Energy, 74, 471-477. https://doi.org/10.1016/j.renene.2014.07.052.

Pasquier, P., & Marcotte, D. (2012). Short-term simulation of ground heat exchanger with an improved TRCM. Renewable Energy, 46, 92-99. https://doi.org/10.1016/j.renene.2012.03.014.

Patankar, S. (1980). Numerical Heat Transfer and Fluid Flow, McGraw-Hill.

Paul, N. D. (1996). The effect of grout thermal conductivity on vertical geothermal heat exchanger design and performance. Master's Thesis. South Dakota University.

Rees, S. J. (2015). An extended two-dimensional borehole heat exchanger model for simulation of short and medium timescale thermal response. Renewable Energy, 83, 518-526. https://doi.org/10.1016/j.renene.2015.05.004.

Rees, S.J., & M. He. (2013). A three-dimensional numerical model of borehole heat exchanger heat transfer and fluid flow, Geothermics, 46, 1-13. doi.org/10.1016/j.geothermics.2012.10.004.

Salim Shirazi, A., & Bernier, M. (2014). A small-scale experimental apparatus to study heat transfer in the vicinity of geothermal boreholes. HVAC&R Research, 20(7), 819-827. doi:10.1080/10789669.2014.939553

Shirazi, A. S., & Bernier, M. (2013). Thermal capacity effects in borehole ground heat exchangers. Energy and Buildings, 67, 352-364. http://dx.doi.org/10.1016/j.enbuild.2013.08.023.

Tarnawski, V. R., Momose, T., Leong, W. H., Bovesecchi, G., & Coppa, P. (2009). Thermal Conductivity of Standard Sands. Part I. Dry-State Conditions. International Journal of Thermophysics, 30(3), 949-968. doi:10.1007/s10765-009-0596-0.

Thorén, Å. (2016). Practical evaluation of borehole heat exchanger models in TRNSYS, M.Sc. Thesis, KTH.

Verstraete, A. (2013). Étude d'une communauté solaire avec stockage thermique saisonnier par puits géothermiques, M.A.Sc. thesis, École Polytechnique de Montréal. https://publications.polymtl.ca/1072/.

Wetter, M., & Huber, A. (1997). TRNSYS Type 451: Vertical Borehole Heat Exchanger EWS Model, Version 3.1-Model Description and Implementing into TRNSYS. Transsolar GmbH, Stuttgart, Germany.

Xu, X., & Spitler, J. D. (2006). Modeling of Vertical Ground Loop Heat Exchangers with Variable Convective Resistance and Thermal Mass of the Fluid. Proceedings of the 10th Int. Conference on Thermal Energy Storage-Ecostock 2006, Pomona, NJ.

Yang, Y., & Li, M. (2014). Short-time performance of composite-medium line-source model for predicting responses of ground heat exchangers with single U-shaped tube. International Journal of Thermal Sciences, 82, 130-137. https://doi.org/10.1016/j.ijthermalsci.2014.04.002.

Yavuzturk, C. and J.D. Spitler. (1999). A short time step response factor model for vertical ground loop heat exchangers. ASHRAE Transactions. 105(2): 475-485.

Zarrella, A., Scarpa, M., & De Carli, M. (2011a). Short time step analysis of vertical ground-coupled heat exchangers: The approach of CaRM. Renewable Energy, 36(9), 2357-2367. doi:10.1016/j.renene.2011.01.032

Zarrella, A., Scarpa, M., & De Carli, M. (2011b). Short time-step performances of coaxial and double U-tube borehole heat exchangers: Modeling and measurements. HVAC&R Research, 17(6), 959-976. https://doi.org/10.1080/10789669.2011.623501.